Supporting information

Photothermal CO₂ hydrogenation to hydrocarbons over trimetallic Co-Cu-Mn catalysts

Zhen-Hong He,[a,]* Zhu-Hui Li,[a] Zhong-Yu Wang,[a] Kuan Wang,[a] Yong-Chang Sun,[a] Sen-Wang Wang,[b] Weitao Wang,[a] Yang Yang,[a] Zhao-Tie Liu[a,b,]*

[a]Shaanxi Key Laboratory of Chemical Additives for Industry, College of Chemistry and Chemical Engineering, Shaanxi University of Science & Technology, 710021 Xi'an, China

[b]School of Chemistry & Chemical Engineering, Shaanxi Normal University, 710119 Xi'an, China

*Corresponding author: hezhenhong@sust.edu.cn (Zhen-Hong He), ztliu@snnu.edu.cn (Zhao-Tie Liu)

Experimental section

Materials

Co(NO$_3$)$_2$·6H$_2$O (99%) was obtained from Aladdin, Cu(NO$_3$)$_2$·3H$_2$O (99%) was obtained from Adamas-Beta, and Mn(NO$_3$)$_2$·4H$_2$O (98%) was provided by Alfa Aesar, respectively. Na$_2$CO$_3$ (≥99.5%) was purchased from Macklin. CO$_2$ (99.999%) and H$_2$ (99.999%) were provided by Jining Xieli Special Gas Co., Ltd. All the other chemicals were obtained from commercial resources and used without purification.

Catalyst preparation

The trimetallic catalysts were prepared by a simple co-precipitation method followed by a partial reduction in H$_2$. Taking the Co$_7$Cu$_1$Mn$_1$O$_x$(200) catalyst as an example, the prepared procedures are as follows. Co(NO$_3$)$_2$·6H$_2$O (1.02 g, 3.5 mmol), Cu(NO$_3$)$_2$·3H$_2$O (0.12 g, 0.5 mmol), and Mn(NO$_3$)$_2$·4H$_2$O (0.126 g, 0.5 mmol) were dissolved in 20 mL of deionized water under continuous stirring for 1 h, and the obtained solution was dropped slowly (about 1 drop per second) into 100 mL of Na$_2$CO$_3$ solvent (0.5 M). Meanwhile, the precipitate was formed and the mixture was stirred for another 10 h at ambient temperature. After stirring for 10 h, the solid was centrifuged (7000 r/min, 5 min) and washed with deionized water until the pH of the filtrate became neutral. Following that, the solid was calcined in a muffle furnace in air at 500 °C (5 °C/min) and maintained at 500 °C for 3 h. The catalyst was further reduced at 200 °C for 2 h with a heating rate of 5 °C/min in a pure H$_2$ flow (40 mL/min). Upon completion of reduction, the catalyst was passivated at ambient temperature in the flow of 1% O$_2$/N$_2$ for 30 min. Finally, the solid catalyst was obtained and denoted as Co$_7$Cu$_1$Mn$_1$O$_x$(200), in which 200 means the reduction temperature. The other monometallic, bimetallic, and trimetallic catalysts with different molar ratios were prepared by the similar procedures but of different feed amounts and reduction temperatures.

Catalyst characterization

The obtained catalysts were characterized by inductively Coupled Plasma-Atomic Emission Spectroscopy (ICP-AES) techniques, N$_2$ adsorption/desorption tests, X-ray diffraction (XRD), (high-resolution) transmission electron microscopy (HR)TEM, X-ray photoelectron spectroscopy (XPS), *etc*. X-ray diffraction (XRD) patterns were recorded on a Rigaku D/max 2500 with nickel

filtered Cu Kα (λ=0.154 nm) at 40 kV and 20 mA with a scanning rate of 10 º/min. The TEM images of the samples were obtained using Talos F200x transmission electron microscopy (Thermo Fisher). The N_2 adsorption/desorption tests were carried out on a Micromeritics ASAP 2460. Prior to the tests, the samples were degassed at 200 ºC for 15 h under vacuum (lower than 0.1 mbar). The surface areas of samples were obtained from the Brunauer-Emmett-Teller (BET) model, and the pore sizes were analyzed by the Barrett-Joyner-Halenda (BJH) method based on the N_2 adsorption/desorption isotherms. The XPS measurements were carried out on a K-Alpha XPS spectrometer (Thermo Fisher Scientific) using Al Kα as the excitation source (hv = 1486.6 eV) and operated at 15 kV and 20 mA.

H_2-TPR and CO_2-TPD tests were analyzed on an Autochem II 2920 instrument. In the H_2-TPR tests, the unreduced samples (20 mg) were preheated to 300 ºC in Ar flow (30 mL/min) and maintained at this temperature for 1 h to remove the adsorbed impurities. After the temperature was cooled to 50 ºC, the gas was switched to 10 vol% H_2/Ar (30 mL/min) and maintained for 60 min. Then the catalyst was heated to 700 ºC with a heating rate of 10 ºC/min, and the consumed H_2 was detected on a TCD detector. In the CO_2-TPD and H_2-TPD tests, the samples were also pretreated at 300 ºC in He (30 mL/min) for 60 min, and then cooled to 50 ºC. The gas was changed to 10 vol% CO_2/He for CO_2-TPD or 10 vol% H_2/He for H_2-TPD tests with a flow rate of 30 mL/min. After 60 min, the remaining CO_2 and H_2 was purged by He gas (30 mL/min) for 60 min, and then was heated to 700 ºC at a rate of 10 ºC/min, and the desorbed CO_2 and H_2 were detected by a TCD detector.

The light intensity was measured by a photoradiometer (PL-MW200, Perfect Light, Beijing, China).

Photoelectrochemical measurements

The photoelectrochemical properties of the samples including EIS Nyquist and Mott-Schottky spectra curves were conducted on a CS2350H electrochemical workstation (Corrtest Instrument Co., Wuhan, China). The three-electrode system contained a working electrode, a Pt foil as the counter electrode, and a standard calomel electrode as the referenced electrode. The working electrode comprised of a conductive glass (15.08 mm×15.08 mm) evenly coated with the catalyst slurry (5 mg of sample and 0.02 mL of Nafion and 0.8 mL of isopropanol), which was dried under vacuum prior to tests.

The photocurrent-time curves were tested at an open circuit test and irradiated by a 300 W Xe lamp in 0.5 mol/L $KHCO_3$ solution. In a typical test, the sample was uniformly covered on an FTO (15.08 mm×15.08 mm).

Photothermal CO_2 reduction

The photothermal CO_2 reduction was carried out in a fixed-bed quartz tube reactor with an internal diameter of about 5 cm and a length of 110 cm, which was equipped with a top-irradiation lamp (300 W, λ = 300-1100 nm, CEL-HXF300, Beijing China Education Au-light Co., Ltd). In the reaction tube, the top of the reaction zone was pressed to a flat plate, and the distance between the lamp with the flat plate is 21 cm (Fig. S1). In a type reaction, 50 mg of catalyst was spread uniformly on a rectangle quartz substrate (4.2 cm × 7.2 cm), which was flatly placed in the reactor tube. After the reactor tube was sealed, the air was evacuated by using a mechanical pump and then the mixed gas of $CO_2/H_2/N_2$ with the molar ratio of 10%/30%/60% was charged to atmosphere pressure. Prior to heating, the Xe lamp light was turned on to heating the catalyst level. Once the temperature maintained stable, the electric heater started to work to enhance the temperature to the set value. Upon the reaction completion, the hydrocarbons in effluent gas were analyzed by a GC (GC9790II, Zhejiang Fuli Analytical Instrument Co., Ltd) with FID and TCD detectors, and the produced CO was detected by a GC (GC9790II) with a methanator with an FID detector. The obtained products were identified by the standard chemicals.

To detect whether the liquids products were obtained, a flowing reaction was conducted for 9 h. The reaction conditions were the same as those of entry 8 in Table 1. The reaction gas passed through the catalyst with a flow rate of 30 ml/min, and was then collected by a condenser with a mixture of cold water and cyclohexane. After reaction, the water and cyclohexane were analyzed on GC to detect whether alcohols and C_{5+} hydrocarbons were produced.

The reusability study of $Co_7Cu_1Mn_1O_x$

The reusability study of the $Co_7Cu_1Mn_1O_x$(200) catalyst was carried out as follows. Upon completion of each photothermal reaction, the reaction gas was analyzed by GC and was then removed under vacuum. After that, the fresh $CO_2/H_2/N_2$ reaction gas was introduced into the reaction, and the following procedures were similar to the above mentioned. For comparison, upon completion

of each photothermal reaction, the photothermal conditions were changed to thermal conditions by turning off the light for the subsequent reactions.

Temporal stability study in continuous-flow reactor

The study for the temporal stability of the $Co_7Cu_1Mn_1O_x(200)$ catalyst was conducted in the same fixed-bed quartz tube reactor. The catalyst (50 mg) was flatly tiled on the quartz substrate, which was placed into the reactor tube. The gas mixture of CO_2, H_2, and N_2 was introduced to the reactor with a ratio of 10%/30%/60%, and the total gas flow rate was 20 mL/min. The effluent gas was analyzed by the GC mentioned above.

Table S1. Photothemal CO_2 reduction over different developed catalysts.

Entry	Catalysts	Temp. (ºC)	Reaction gases	Light	Activity (mmol·g_{cat}^{-1}·h^{-1}) CO	CH$_4$	C$_{2+}$	Ref.
1	Ru/Mg-Al LDHs matrix (Ru@FL-LDHs)	350	CO_2/H_2 (5.0/20.5 mL/min)	300 W Xe lamp		277 (in a flow-type reaction system)		[1]
2	RuO_2/$SrTiO_3$	150	CO_2/H_2 (0.25 bar/1.05 bar)	300 W Xe lamp		14.6		[2]
3	RuO_2/3D silicon photonic crystals	Ambient temperature	CO_2/H_2 (1/4)			4.4		[3]
4	Ru/TiO_2	300	CO_2/H_2 (1/3) 10 mL/min	1.5 G sunlight		69.49		[4]
		150				1.72		
5	Ru/silicon nanowire	150	CO_2/H_2 (1/4, 45 psi)			about 1.0	0	[5]
6	Ru/Al_2O_3	370	CO_2/H_2 (CO_2, 2-2.05 mmol; H_2 8.2-8.5 mmol)		0.14	18.0		[6]
7	Pd@Nb_2O_5 (large Pd)			300 W Xe lamp	0.75 (mol·g_{Pd}^{-1}·h^{-1})	0.11 (mol·g_{Pd}^{-1}·h^{-1})		[7]
8	Pd@Nb_2O_5 (small Pd)			300 W Xe lamp	18.8 (mol·g_{Pd}^{-1}·h^{-1})			[7]
9	Ni/SiO_2.Al_2O_3	<150	CO_2/H_2/N_2 (15/70/15)	solar simulator	1.4	48.6	0	[8]
11	Cu_2O/Graphene	250	CO_2/H_2 (0.25 bar/1.05 bar) 1.3 bar	300 W Xe lamp	-	14.93 mmol·g_{Cu2O}^{-1}·h^{-1}	-	[9]
12	Cu_2O/Zn-MOFs	215	CO_2/H_2 (0.25 bar/ 1.05 bar)	Xe lamp (300 W)		0.01		[10]
13	1.0%NiO-3%In_2O_3-TiO_2	Ambient temperature	CO_2/H_2/Ar (15/60/25 mL/min)	300 W Xe lamp	0.243	0.208		[11]
14	CoFeAl-LDH nanosheets	about 300	CO_2/H_2/Ar (15/60/25) 0.18 MPa	300 W Xe light	5% (Sel.)	60% (Sel.)	35% (Sel.)	[12]
15	Ni-Al_2O_3/SiO_2	225	CO_2/H_2 (4.41/17.82 ml/min)	UV-Vis 300 W Xe lamp		about 55 uL/min (initial 4 h)		[13]
16	$Co_7Cu_1Mn_1O_x$(200)	200	CO_2/H_2/N_2 (10%/30%/60%)	UV-Vis 300 W Xe lamp	1.1 (6.5%)	14.5 (85.3)	1.4 (8.2%)	This work
17	$Co_7Cu_1Mn_1O_x$(200)	200	CO_2/H_2 (25%/75%)	UV-Vis 300 W Xe lamp	0.9 (3.7%)	15.9 (65.4%)	7.5 (30.9%)	This work
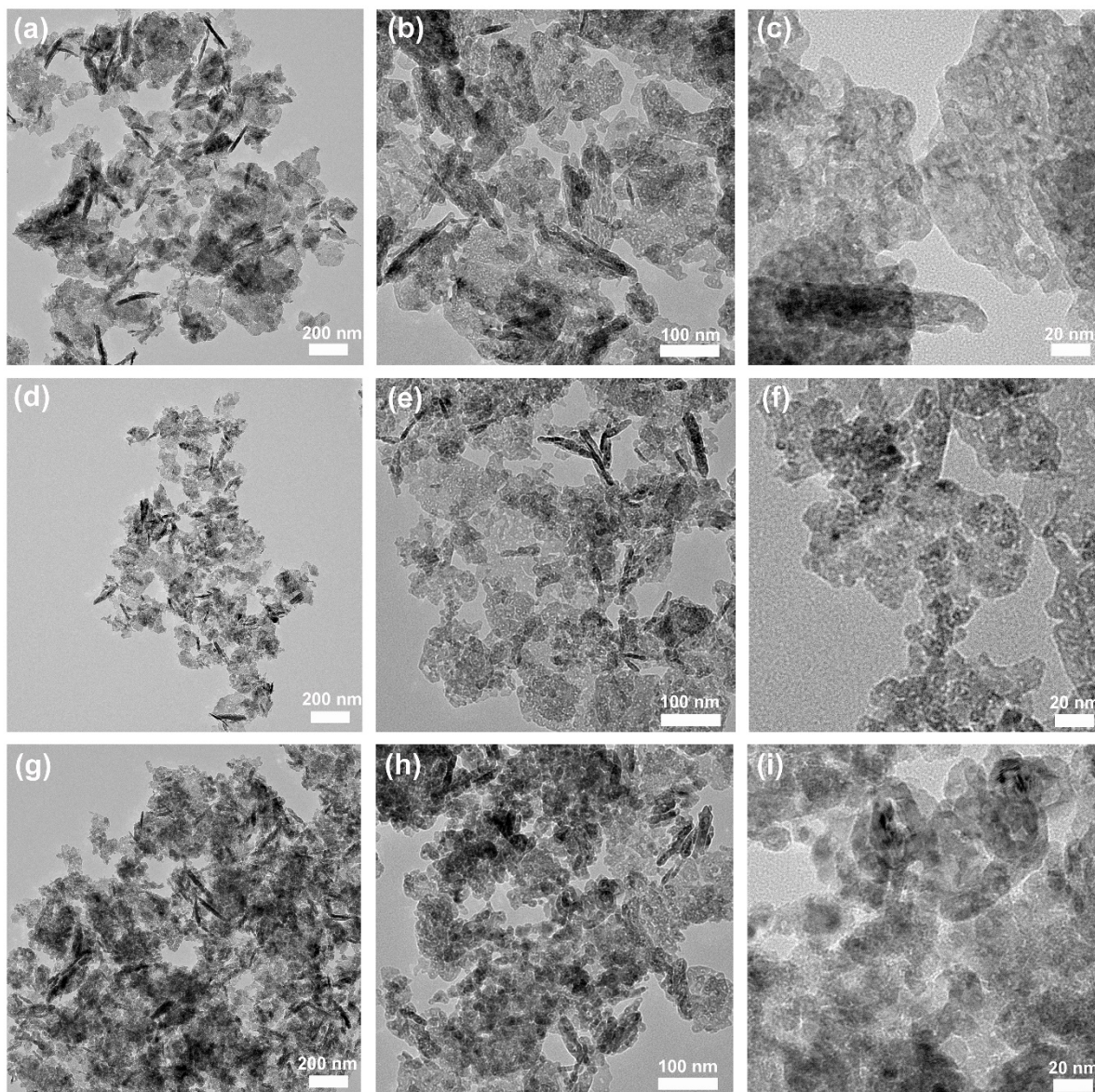
Fig. S1 TEM images of (a-c) $Co_3Cu_1Mn_1O_x(200)$, (d-f) $Co_5Cu_1Mn_1O_x(200)$, and (g-i) $Co_9Cu_1Mn_1O_x(200)$.

Table S2. ICP-OES results of different bimetallic and ternary catalysts.

Entry	Catalysts	Theoretical value[a]	ICP-OES tested
1	$Co_7Mn_1O_x$	$Co_7Mn_1O_x$	$Co_{6.8}Mn_1O_x$
2	$Co_7Cu_1O_x$	$Co_7Cu_1O_x$	$Co_{6.91}Cu_1O_x$
4	$Co_3Cu_1Mn_1O_x$	$Co_3Cu_1Mn_1O_x$	$Co_{2.71}Cu_{0.91}Mn_1O_x$
5	$Co_5Cu_1Mn_1O_x$	$Co_5Cu_1Mn_1O_x$	$Co_{5.13}Cu_{0.93}Mn_1O_x$
6	$Co_7Cu_1Mn_1O_x$	$Co_7Cu_1Mn_1O_x$	$Co_{6.87}Cu_{0.92}Mn_1O_x$
7	$Co_1Cu_3Mn_1O_x$	$Co_1Cu_3Mn_1O_x$	$Co_{0.93}Cu_{3.12}Mn_1O_x$

[a] Calculated from the feed amount of precursor salts.
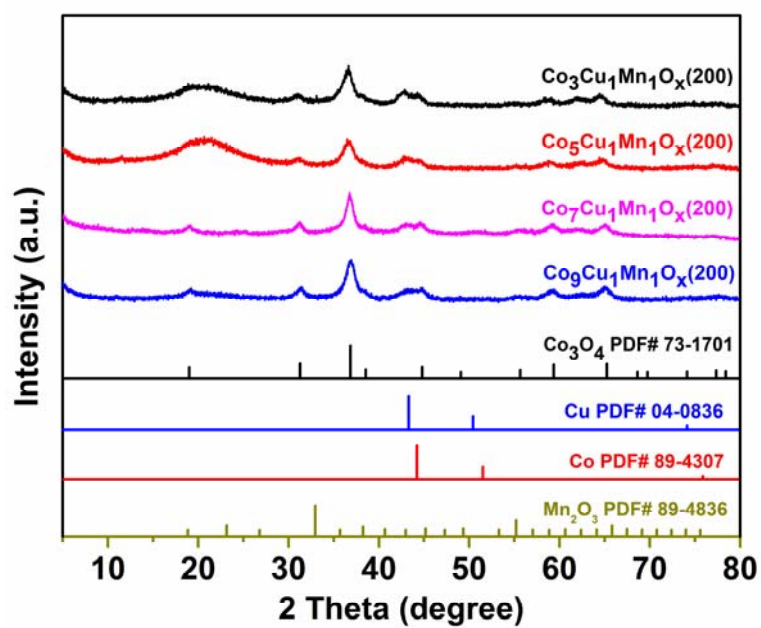
Fig. S2 XRD of the Co-Cu-Mn trimetallic catalysts with different metal molar ratios.
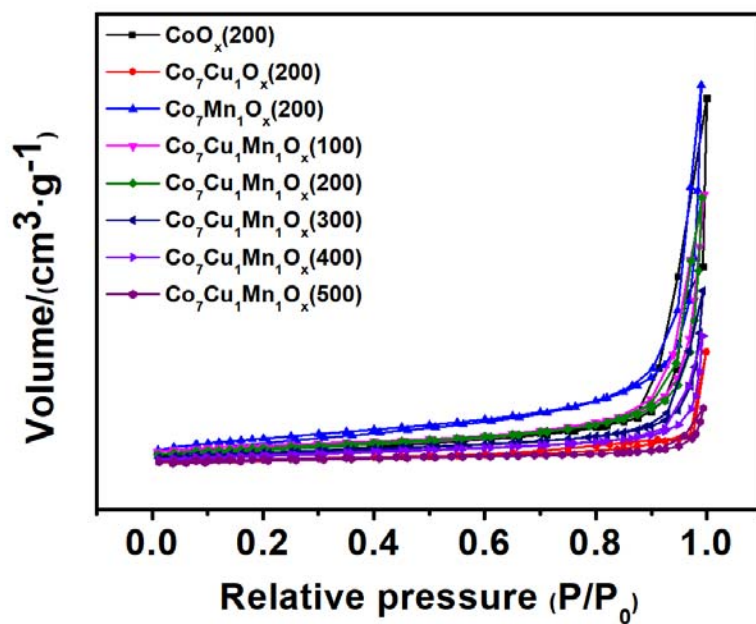
Fig. S3 N_2 adsorption/desorption isotherms for diverse catalysts.

Table S3. The analysis results of N_2 adsorption/desorption isotherms for catalysts.

Entry	Catalyst	BET surface area (m^2/g)	Pore diameter (nm)	Pore volume (cm^3/g)
1	CoO_x(200)	64	16.6	0.34
2	$Co_7Cu_1O_x$(200)	23	15.6	0.16
3	$Co_7Mn_1O_x$(200)	107	22.5	0.65
4	$Co_7Cu_1Mn_1O_x$(100)	72	22.9	0.44
5	$Co_7Cu_1Mn_1O_x$(200)	66	25.7	0.46
6	$Co_7Cu_1Mn_1O_x$(300)	49	23.6	0.30
7	$Co_7Cu_1Mn_1O_x$(400)	39	20.0	0.22
8	$Co_7Cu_1Mn_1O_x$(500)	21	9.8	0.09
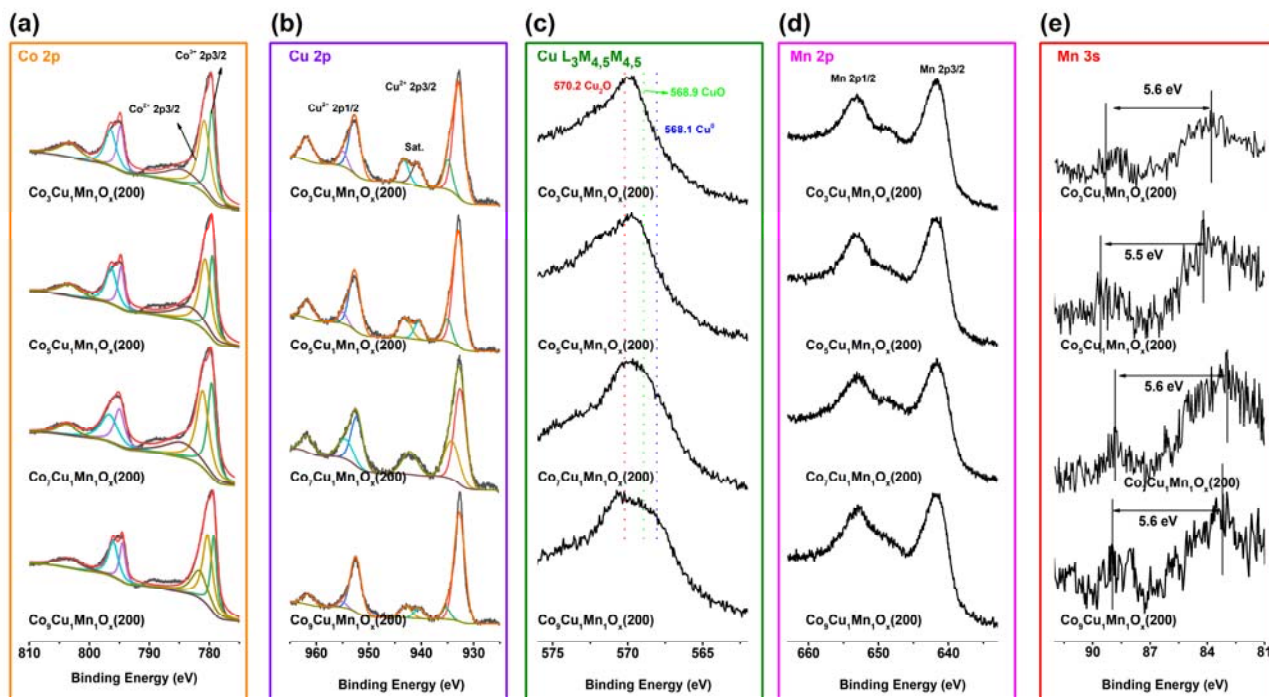
Fig. S4 XPS of the Co-Cu-Mn trimetallic catalysts with different metal molar ratios .
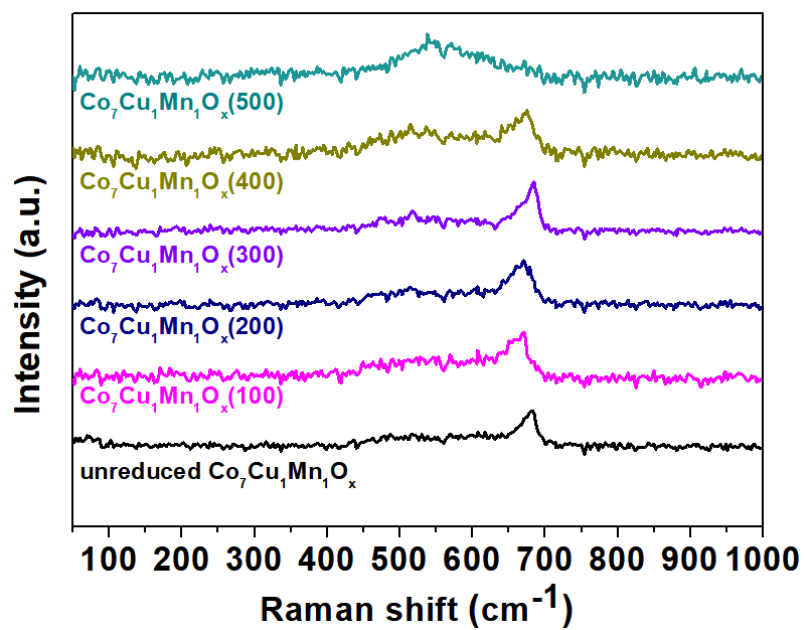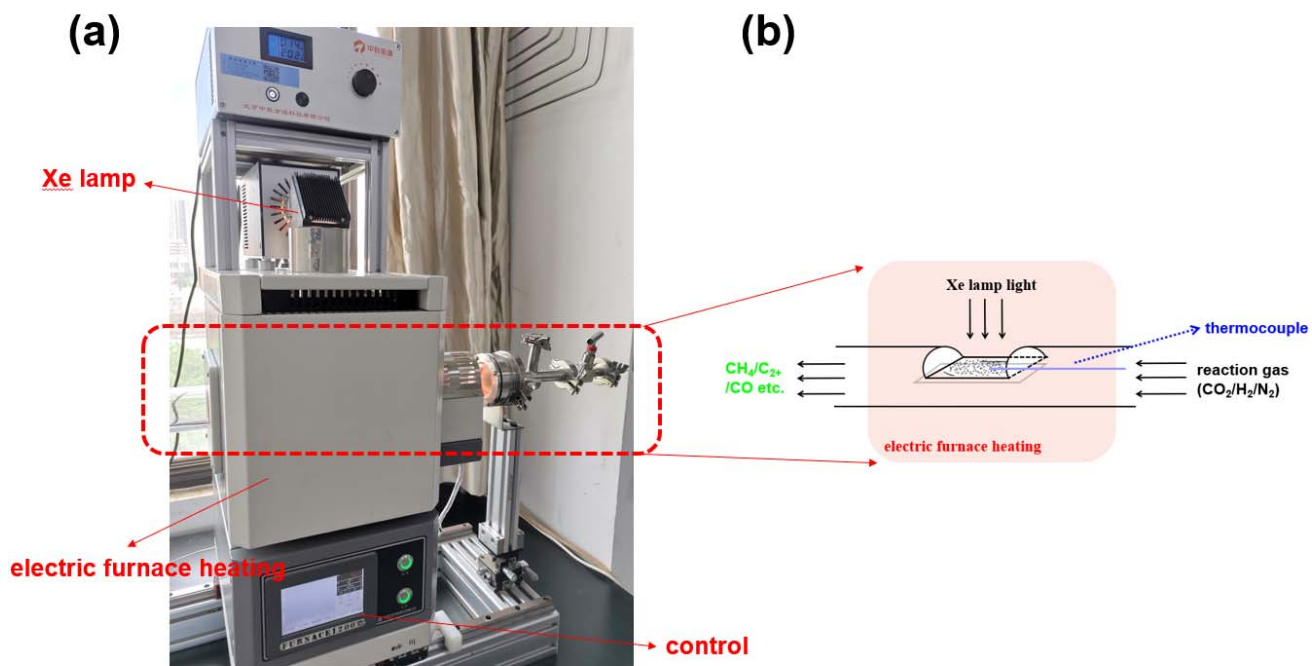
Fig. S5 Raman spectra of different catalysts.

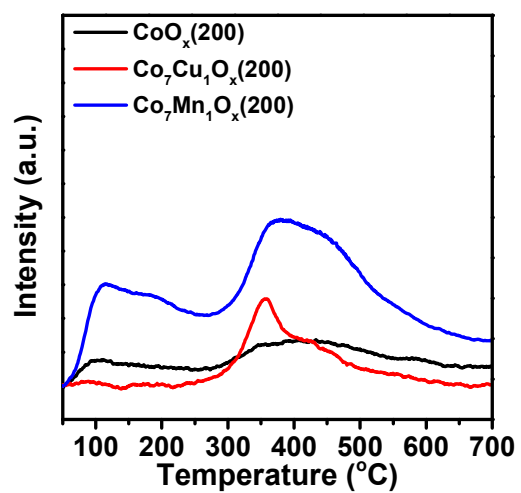Fig. S6 (a) Digital image of equipment for the photothermal CO_2 hydrogenation, and (b) the reaction zone.

(a) CO$_2$-TPD
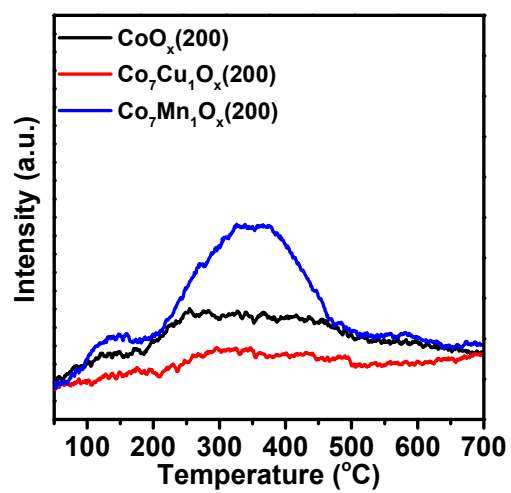
(b) H$_2$-TPD

Fig. S7 CO$_2$-TPD and H$_2$-TPD results for CoO$_x$(200), Co$_7$Mn$_1$O$_x$(200), and Co$_7$Cu$_1$O$_x$(200).

Table S4. Catalytic performances of Co-Cu and Co-Mn bimetallic catalysts.

Entry	Catalyst	CO_2 conv. (%)	Activity (mmol·g_{cat}^{-1}·h^{-1})			CH_4 Sele. (%)
			CH_4	C_{2+}	CO	
1	$Co_7Mn_1O_x$	3.6	0.1±0.1	0.0	2.1±0.1	4.5
2	$Co_7Mn_1O_x(100)$	0.8	0.1±0.1	0.0	0.4±0.1	20.0
3	$Co_7Mn_1O_x(200)$	0.8	0.2±0.1	0.0	0.3±0.1	40.0
4	$Co_7Mn_1O_x(300)$	11.8	5.4±0.2	0.8±0.1	1.1±0.1	74.0
5	$Co_7Mn_1O_x(400)$	16.0	8.1±0.2	0.8±0.1	1.0±0.1	81.8
6	$Co_7Mn_1O_x(500)$	11.8	5.9±0.1	0.6±0.1	0.8±0.1	80.8
7	$Co_7Cu_1O_x$	25.3	9.6±0.2	4.3±0.1	1.8±0.1	61.1
8	$Co_7Cu_1O_x(100)$	17.9	7.1±0.2	3.0±0.1	1.0±0.1	64.0
9	$Co_7Cu_1O_x(200)$	14.0	5.9±0.2	2.4±0.1	0.4±0.1	67.8
10	$Co_7Cu_1O_x(300)$	19.4	7.6±0.1	3.1±0.1	1.3±0.1	63.3
11	$Co_7Cu_1O_x(400)$	18.2	6.7±0.3	3.4±0.1	1.2±0.1	59.3
12	$Co_7Cu_1O_x(500)$	5.3	1.5±0.2	0.0±0.1	1.8±0.1	45.5

[a]Reaction conditions: catalyst 50 mg, CO_2/H_2/N_2 10%/30%/60%, full irradiation, 200 °C, 3 h.

$^{13}CO_2$ isotope labeling experiment

To detect the methane was obtained from the photothermal CO_2 reduction reaction, the $^{13}CO_2$ isotope labeling experiment was carried out under the conditions of entry 8 in Table 1, but added 20 ml of $^{13}CO_2$ gas into the reaction tube. Upon completion of reaction, the reaction gas was analyzed by a mass spectroscopy (HPR20, Hiden Analytical), and the result is given in Fig. S8.
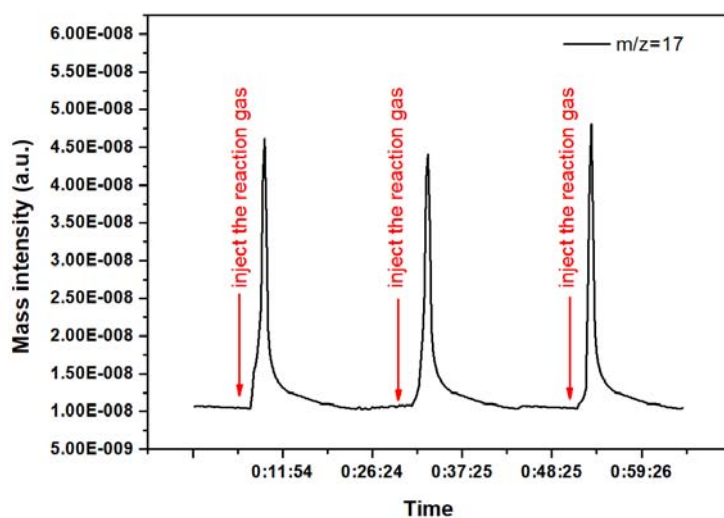

Fig. S8 The signal variation of $^{13}CH_4$ (m/z=17) after injecting the reaction gas obtained from $^{13}CO_2$ isotope labeling experiment.
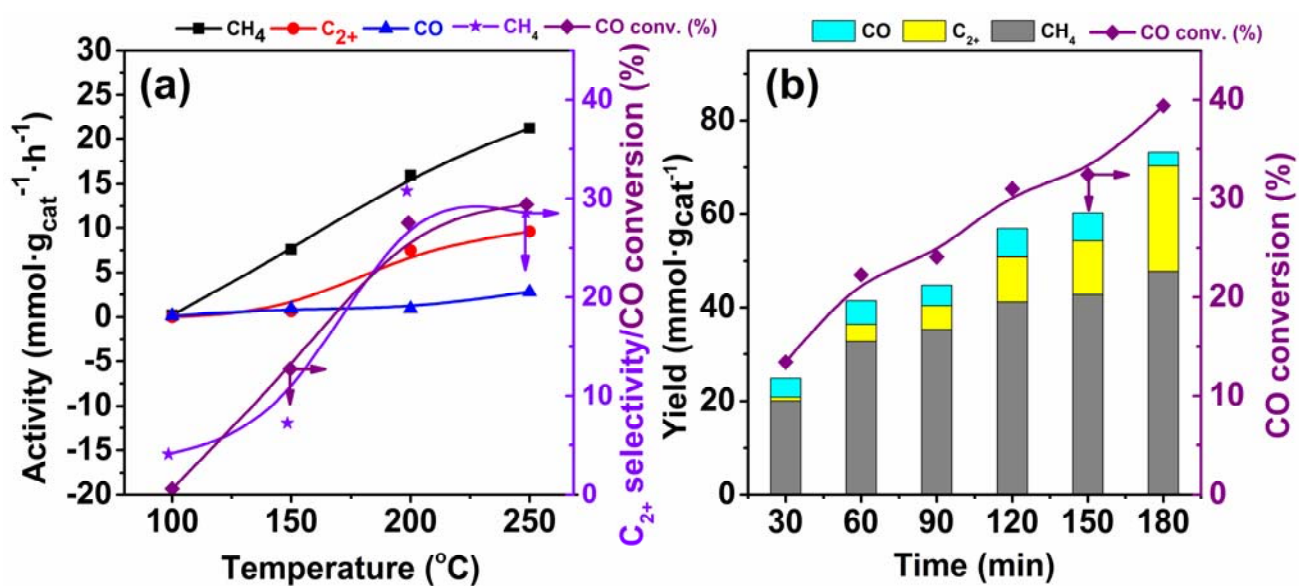
Fig. S9 Effects of reaction temperature (a) and reaction time (b) on the catalytic performances on photothermal CO_2 reduction to C_{2+} hydrocarbons over the $Co_7Cu_1Mn_1O_x$(200) catalyst. Reaction conditions: (a) catalyst 50 mg, 300 W Xe lamp full irradiation, CO_2/H_2 25%/75%, 3 h, and (b) catalyst 50 mg, 300 W Xe lamp full irradiation, CO_2/H_2 25%/75%, 200 °C.
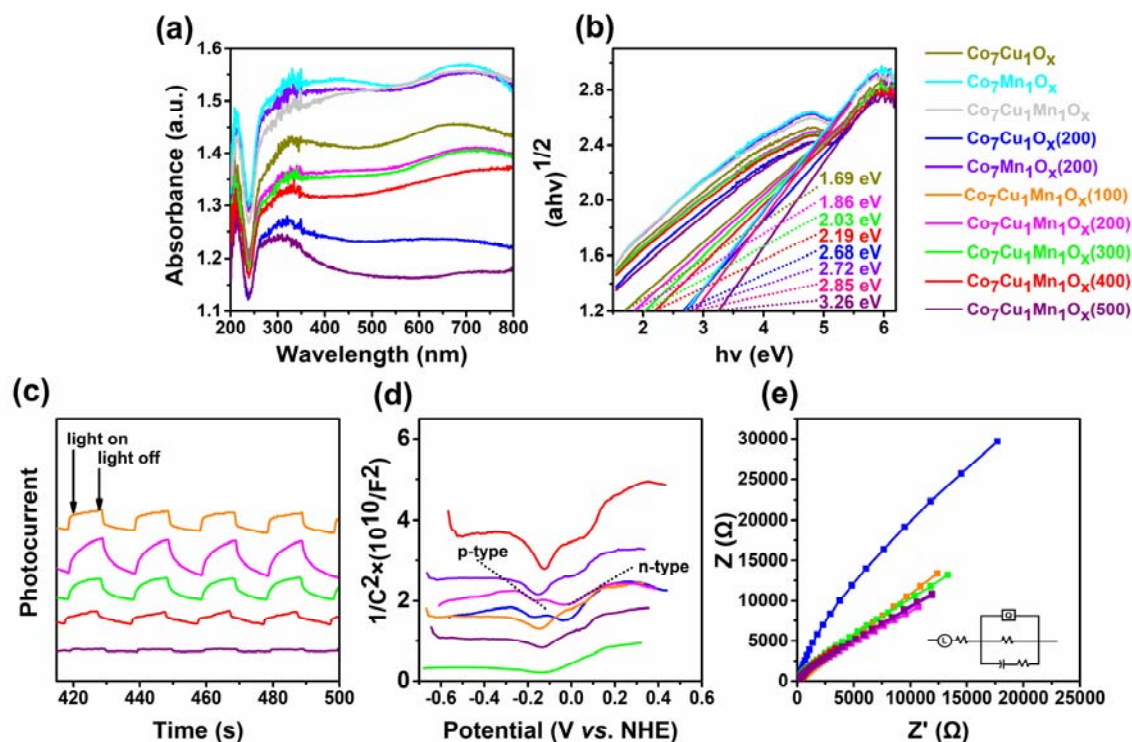
Fig. S10 (a) UV-vis diffuse reflectance spectra for diverse catalysts, (b) corresponding plots for the determination of band gap energy(eV) values. Photo-electrochemical characterizations of (c) photocurrent-time curves, (d) Mott-Schottky curves, and (e) EIS Nyquist plots for various catalysts.

Table S5. Effect of excitation wavelength on photothermal CO_2 hydrogenation over the $Co_7Cu_1Mn_1O_x(200)$ catalyst.[a]

Entry	Light sources	Light powder (mW/cm^2)	CO_2 Con. (%)	Activity (mmol·g$_{cat}^{-1}$·h^{-1})			CH$_4$ Sele. (%)
				CH$_4$	C$_{2+}$	CO	
1	Full irradiation (300-1100 nm)	234	27.4	14.5	1.4	1.1	85.3
2	Visible light (>420 nm)	72	24.9	13.1	1.3	1.0	85.1
3	UV light (300-420 nm)	171	26.1	13.8	1.8	0.6	85.2

[a]Reaction conditions: catalyst 50 mg, $CO_2/H_2/N_2$ 10%/30%/60%, 200 ºC, 3 h.

Catalysts	Temperature (°C)
$CoO_x(200)$	97.7
$CuO_x(200)$	88.3
$MnO_x(200)$	104.6
$Co_7Cu_1Mn_1O_x$ (200)	102.2
$Co_7Cu_1Mn_1O_x$ (500)	95.8

$CoO_x(200)$ 97.7 °C

$Co_7Cu_1Mn_1O_x(200)$ 102.2 °C

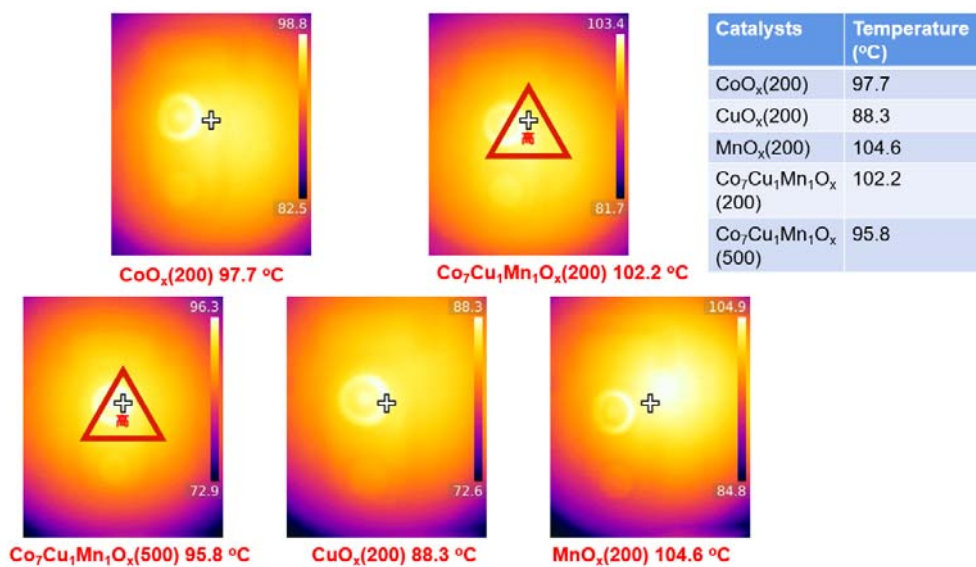$Co_7Cu_1Mn_1O_x(500)$ 95.8 °C

$CuO_x(200)$ 88.3 °C

$MnO_x(200)$ 104.6 °C

Fig. S11 The photothermal effect over different samples under vacuum using an infrared thermal camera.
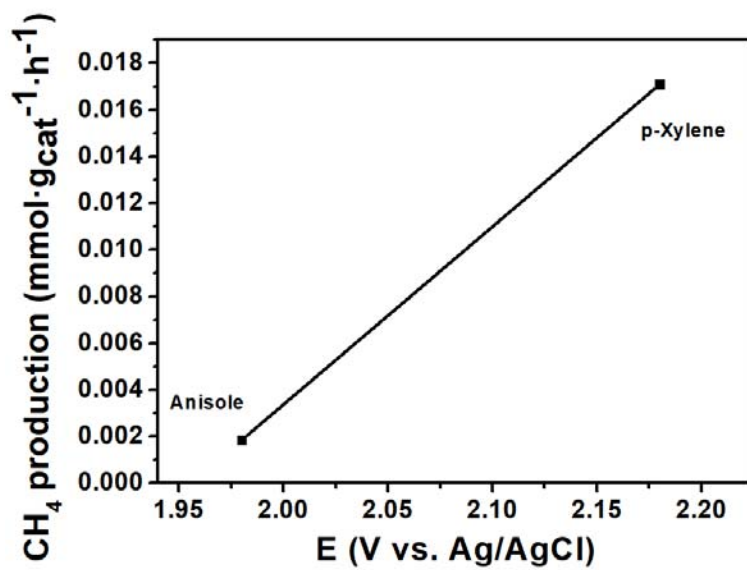
Fig. S12 Results of control experiments by adding anisole and *p*-xylene as sacrificial electron donors.

Table S6. Control experiments of using different reaction gases.[a]

Entry	Reaction gas	CO_2 Con. (%)	Activity (mmol·g_{cat}^{-1}·h^{-1})			Selectivity (%)	
			CH_4	C_{2+}	CO	CH_4	C_{2+}
1[b]	10%CO_2/30%H_2/60%N_2	27.4	14.5	1.4	1.1	85.3	8.2
2	10%CO/30%H_2/60%N_2	19.7	4.9	7.3	-	40.2	59.8
3[c]	2%CO /8%CO_2/30%H_2/60%N_2	16.1	7.2	2.8	-	72.0	28.0

[a]Other reaction conditions are similar to those of Table 1, entry 8. [b]Copied from entry 8 in Table 1.

[c]The selectivity did not contain the CO generated from CO_2.
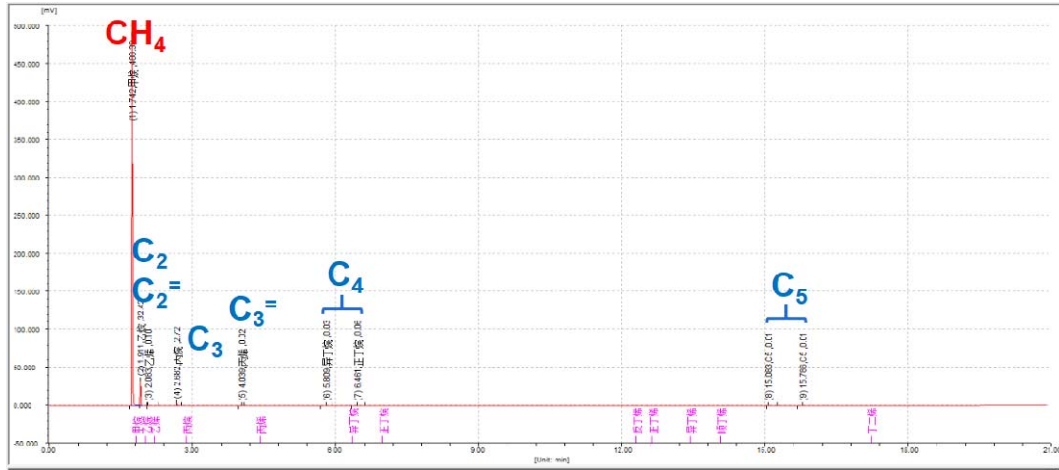
Fig. S13 GC spectrum of CH$_4$ and C$_{2+}$ hydrocarbons obtained from the conditions of entry 8 in Table 1.
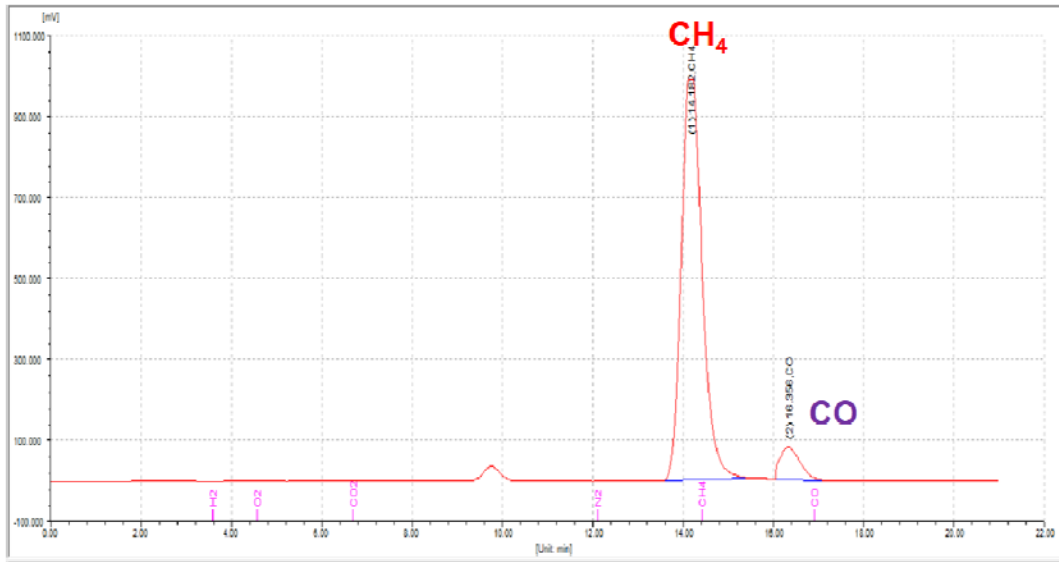

Fig. S14 GC spectrum of CO obtained from the conditions of entry 8 in Table 1.
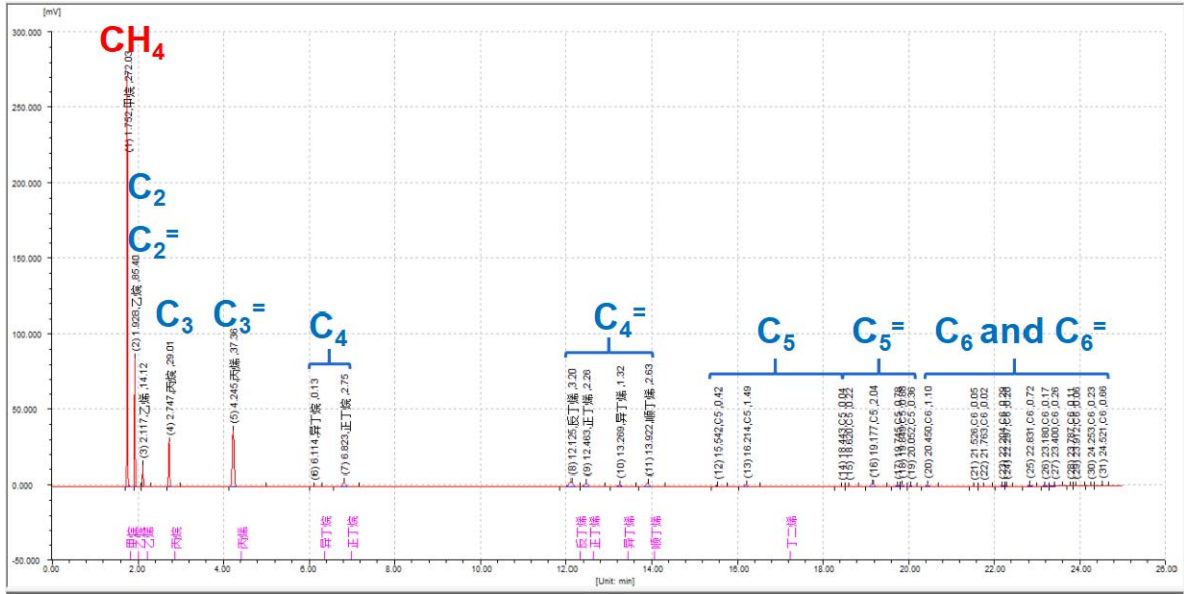
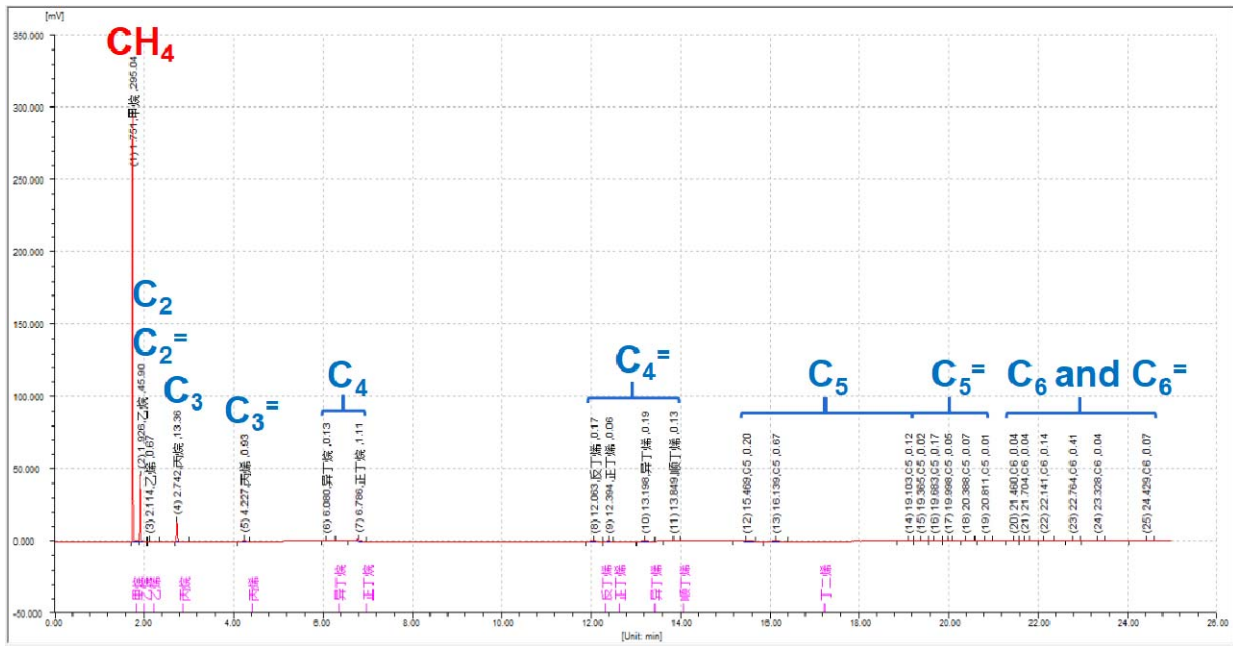Fig. S15 GC spectrum of hydrocarbons obtained from the conditions of entry 2 in Table S6.

Fig. S16 GC spectrum of hydrocarbons obtained from the conditions of entry 3 in Table S6.
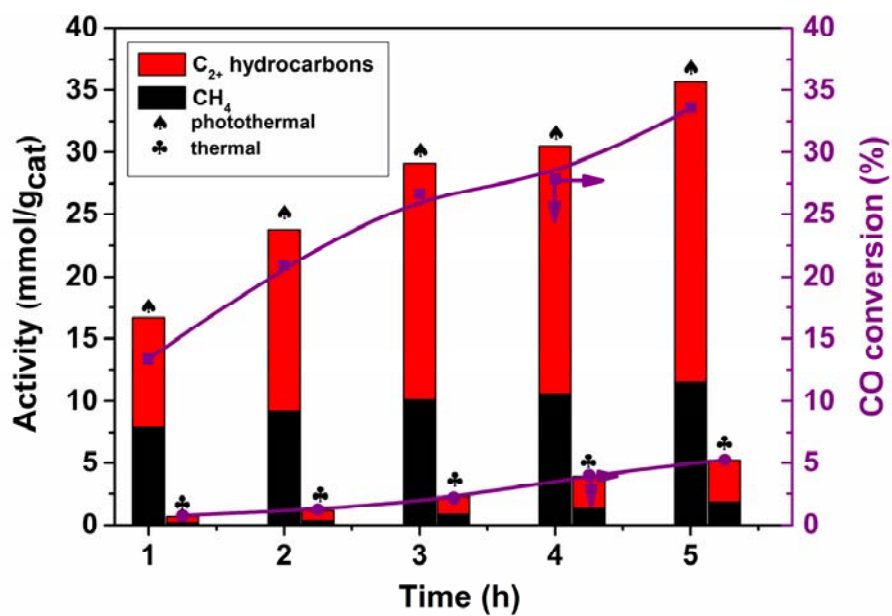
Fig. S17 Photothermal and thermal F-T synthesis over the $Co_7Cu_1Mn_1O_x(200)$ catalyst. Reaction conditions: catalyst 50 mg, 200 ºC, $CO/H_2/N_2$ 10%/30%/60%, 300 W Xe lamp full irradiation.
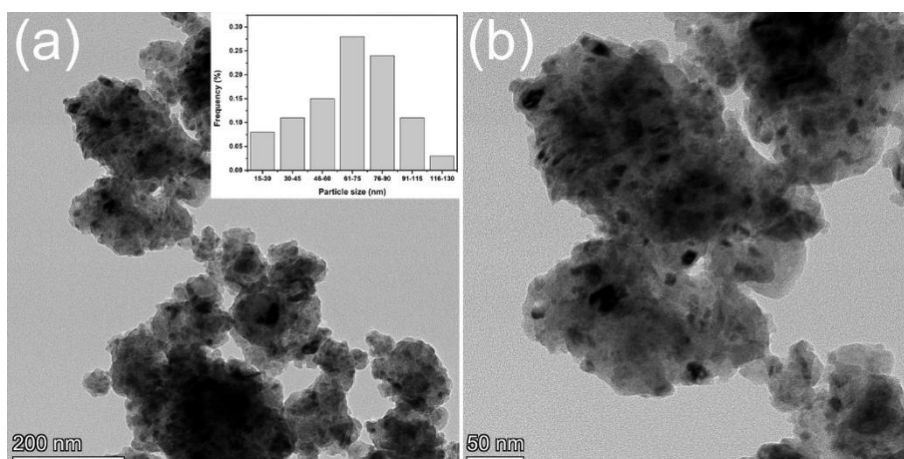
Fig. S18 The TEM image of the catalyst after 18 uses.

References

[1]   J. Ren, S. Ouyang, H. Xu, X. Meng, T. Wang, D. Wang, J. Ye, *Adv. Energy Mater.*, 2016, 1601657.

[2]   D. Mateo, J. Albero, H. García, *Joule*, 2019, 3, 1-14.

[3]   A.A. Jelle, K.K. Ghuman, P.G. O'Brien, M. Hmadeh, A. Sandhel, D.D. Perovic, C.V. Singh, C.A. Mims, G.A. Ozin, *Adv. Energy Mater.*, 2018, 8, 1702277.

[4]   C. Wang, S. Fang, S. Xie, Y. Zheng, Y.H. Hu, *J. Mater. Chem. A*, 2020, 8, 7990-7394.

[5]   P.G. O'Brien, A. Sandhel, T.E. Wood, A.A. Jelle, L.B. Hoch, D.D. Perovic, C.A. Mims, G.A. Ozin, *Adv. Sci.*, 2014, 1, 1400001.

[6]   X. Meng, T. Wang, L. Liu, S. Ouyang, P. Li, H. Hu, T. Kako, H. Iwai, A. Tanaka, J. Ye, *Angew. Chem. Int. Ed.*, 2014, 53, 11478–11482

[7]   J. Jia, H. Wang, Z. Lu, P.G. O'Brien, M. Ghoussoub, P. Duchesne, Z. Zheng, P. Li, Q. Qiao, L. Wang, A. Gu, A.A. Jelle, Y. Dong, Q. Wang, K.K. Ghuman, T. Wood, C. Qian, Y. Shao, C. Qiu, M. Ye, Y. Zhu, Z.-H. Lu, P. Zhang, A.S. Helmy, C.V. Singh, N.P. Kherani, D.D. Perovic, G.A. Ozin, *Adv. Sci.*, 2017, 1700252.

[8]   F. Sastre, A.V. Puga, L. Liu, A. Corma, H. García, *J. Am. Chem. Soc.*, 2014, 136, 6798–6801.

[9]   D. Mateo, J. Albero, H. García, *Energy Enviorn. Sci.*, 2017, 10, 2392–2400.

[10]   M. Cabrero-Antonino, S. Remiro-Buenamañana, M. Souto, A.A. García-Valdivia, D. Choquesillo-Lazarte, S. Navalón, A. Rodríguez-Diéguez, G.M. Espallargas, H. García, *Chem. Commun.*, 2019, 55, 10932–10935.

[11]   M. Tahir, B. Tahir, N.A.S. Amin, A. Muhammad, *Energy Convers. Manag.*, 2016, 119, 368–378.

[12]   G. Chen, R. Gao, Y. Zhao, Z. Li, G.I.N. Waterhouse, R. Shi, J. Zhao, M. Zhang, L. Shang, G. Sheng, X. Zhang, X. Wen, L.-Z. Wu, C.-H. Tung, T. Zhang, *Adv. Mater.*, 2017, 1734663.

[13]   J. Albero, E. Dominguez, A. Corma, H. García, *Sustain. Energ. Fuels*, 2017, 1, 1303–1307.